Control of cavity-driven separated boundary layer

J. Hœpffner[1], E. Åkervik[1], U. Ehrenstein[2] and D. S. Henningson[1]

[1] KTH Mechanics, S-100 44 Stockholm, Sweden
[2] Laboratoire J.A. Dieudonné, Parc Valrose; F-06108 Nice Cedex 02, France

Summary

The aim of this paper is to build a reduced model for control design based on the eigenmodes of the 2D cavity flow. The flow dynamics is dominated by the shear layer instability, and the pressure is found to play a coupling role between separation and re-attachment, potentially leading to global instability. The large dimensionality of the discretized flow system is a challenge for control design. A reduced dynamic model is constructed by projection on a basis of eigenmodes, and a controller is computed based on this reduced model.

1 Introduction

Active flow control has received increasing attention in the last decade, where knowledge from fluid mechanics is combined with control theory to affect the properties of flow systems. A common goal is to stabilize a flow subject to linear instability, like for instances the Tollmien-Schlichting waves on an aeroplane wing (see e.g. Högberg & Henningson (2002)), or force the flow back to a laminar regime, like for instance in a turbulent channel flow (see e.g. Högberg *et al.* (2003*a*); Kim (2003)).

These systems are described by partial differential equations. These can be discretized in time and space and typically lead to large systems of ordinary differential equations. This represents a challenge for control design based on optimization methods like the linear quadratic Gaussian (LQG) method, or more recently the $\mathcal{H}_2$ and $\mathcal{H}_\infty$ control synthesis. On the other hand, many flow cases exhibit low dimensionality. For instance, only one eigenmode might be unstable, so that one can hope to describe properly the flow's dynamics with a simpler dynamical system. It is thus preferable to first build a reduced order model for the flow system. This is typically a heavy computational task, but once this model is obtained, one has the possibility to experiment with many control strategies and set of control parameters to obtain the desired flow behaviour. The final test is to apply the controller thus designed on the original flow system. As a first step, in the present analysis the controller built for a drastically reduced system is applied to the high-dimensional dynamical system.

Several techniques are available for model order reduction, the most widely used of which are the balanced truncation or the optimal Hankel norm minimization (see e.g. Obinata & Anderson (2001)). But these are computationally intensive and cannot readily be implemented in large scale systems. One the other hand, thanks to increasing computational power and the use of Arnoldi method (see Edwards *et al.* (1994)), it has now become possible to solve large eigenvalue problems, i.e. including the eigenanalysis of a complete two dimensional flow. These eigenmodes can in turn be used as a reduced basis for the Galerkin projection of the flow dynamics. Hopefully, a small family of the eigenmode can represent correctly the target flow dynamics. For a review of eigenmodes analysis with several dimensions in fluid mechanics, see e.g. Theofilis (2003).

In this paper, we aim at controlling the instability in an open cavity in a boundary layer. This flow presents similarities to the separated boundary layer where the recirculation is induced by an adverse pressure gradient. In the case of the cavity, the recirculation bubble is due to the wall curvature. This flow present as well some similarities to the rectangular cavity extensively studied for the generation of strong acoustic noise (see e.g. Rowley *et al.* (2002)). The central element of this recirculated flows is the shear layer, i.e. the region of large shear that isolates the recirculating zone from the free-stream. It is subject to large growth due to Kelvin–Helmholtz instability (see Huerre (2000)).

2 Description of the geometry

A cavity with smooth edges, or *lips*, and a large aspect ratio, as seen in figure 1 is considered. The presence of the cavity induces a separated region, isolated from the free-stream by a shear layer. At the end of the cavity, the *downstream cavity lip*, the flow re-attaches, and slowly relaxes downstream to a flat plate boundary layer again. The Reynolds number based on the displacement thickness at inflow and the free-stream velocity, was chosen such that the boundary layers upstream and downstream of the cavity are stable to Tollmien-Schlichting waves, so that the flow is dominated by the effect of the cavity.

3 Numerical tools

The base flow is obtained by means of direct numerical simulation (DNS) of the nonlinear Navier-Stokes system. The base flow thus obtained is interpolated on a spectral grid for computation of the eigenmodes. We choose a spectral spatial discretization, which is optimal in terms of accuracy, for the eigenmode computation in order to reduce the memory requirement. Once the eigenmodes computed, we can use them as a reduced order model for
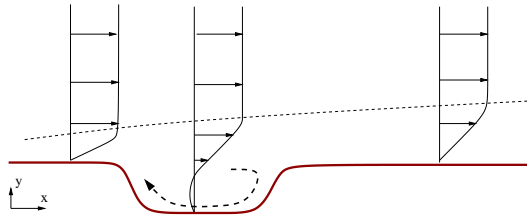
Figure 1   Sketch of the geometry, with Blasius boundary layers upstream and downstream of the domain, with recirculation inside the cavity. The recirculating region is isolated from the free-stream by a shear layer.

the system. We will use this model to analyse the possible energy growth mechanisms, and then for control design optimization.

The numerical solution procedure to solve the Navier–Stokes system in this highly non parallel geometry has previously been considered for bump-like geometries triggering boundary-layer separation (Marquillie & Ehrenstein (2003)). We use a coordinate transformation to account for the wall curvature. Fourth-order finite differences are used in the streamwise x-direction, whereas the wall-normal y-direction is discretized using Chebyshev-collocation. Second-order backward Euler differencing is used in time: the Cartesian part of the diffusion term is taken implicitly whereas the nonlinear and metric terms are evaluated using an explicit second-order Adams-Bashforth scheme. In order to ensure a divergence-free velocity field a fractional time-step procedure has been adapted to the present formulation of the Navier–Stokes system with coordinate transformation.

A streamwise length $L = 400$ has been considered, the cavity geometry being confined between $x \approx 30$ and $x \approx 150$. The distance between the cavity and the end of the computational domain is large enough for the flow dynamics in the vicinity of the cavity to be independent of possible reflections at outflow. Up to 3000 grid points in x have been considered with up to 129 collocation points in the wall-normal direction.

To compute the base flow, we initiate the computational domain with zero velocity, and enforce the boundary conditions, that is uniform free-stream flow at infinity, the Blasius profile at inflow and no-slip at the wall. The flow is then marched in time until a stationary state is obtained. In cases of a globally unstable base flow, a time domain filtering technique is used to reach the unstable steady state.

Once a steady state $\mathbf{U}(x,y) = (U(x,y), V(x,y))$ is obtained, the Navier-Stokes system is linearized considering a disturbance in the flow field and pressure as used in Ehrenstein & Gallaire (2005) for the computation of global modes for the weakly non-parallel flat-plate boundary layer flow.

The eigenvalue problem obtained after discretization may be written formally as

$$-i\omega \mathbf{B} \, \mathbf{q} = \mathbf{A} \, \mathbf{q} \qquad (1)$$

the vector $\mathbf{q}$ containing the discretized disturbance flow velocity and pressure, $-i\omega$ being the generalized eigenvalue. In the forthcoming analysis up to 250 collocation points in x and 65 collocation points in y have been considered and hence more than 48 000 complex equations. Such a system is too large to be solved by standard QZ algorithms and Krylov subspace projections provide the possibility to recover part of the spectrum using the "shift and invert" strategy. Details of the method are given for instance in Nayar & Ortega (1993). The complexity reduces to the computation of the Krylov subspace together with the Arnoldi algorithm: Introducing a shift parameter λ, the Krylov subspace may be computed by a successive resolution of linear systems with matrix $(\mathbf{A} - \lambda \mathbf{B})$, using a LU decomposition, which is achievable even for a very large matrix (cf Ehrenstein & Gallaire (2005)). A large part of the spectrum can be recovered when considering a large Krylov subspace. Here, we considered reduced systems, the eigenvalues being determined using a QZ-algorithm, with up to $m = 800$ equations. The operator is shifted in order to provide the spectrum in a neighbourhood of the shift parameter λ. In most of the computations we set $\lambda = 0$. Given the large Krylov subspace we considered, the part of the spectrum relevant for our analysis could be recovered in one computation. Projection on the global modes are achieved using the bi-orthogonality condition involving the adjoint modes.

3.1   Computation of the optimal initial condition

To exhibit the rich behaviour of the cavity flow, we compute the initial flow condition that leads to the largest energy growth. The possibility of initial transient energy growth is related to to the non-normality of the governing operator, i.e. to the non-normality of its eigenvectors. This transient energy amplification is also refereed to as *non-modal* since it is not due to the behaviour of a single eigenmode, but is caused by the superposition of several of them. For precise description of the procedure, see Schmid & Henningson (2001).

4   Base flow and Eigenmodes of the cavity flow

4.1   Description of the base flow

The obtained steady flow is depicted in figure 2. It is a steady solution of the Navier–Stokes equation for the cavity geometry at Reynolds number 350. We can observe the Blasius boundary layers upstream and downstream of the cavity. The main effect of the cavity is the generation of the recirculation zone and the shear layer. It can be seen on this figure that the shear layer

slowly diffuses and extends in the y direction. We can observe the inflection points of the shear layer. This is the origin of the shear layer instability that plays a strong role in the cavity dynamics.
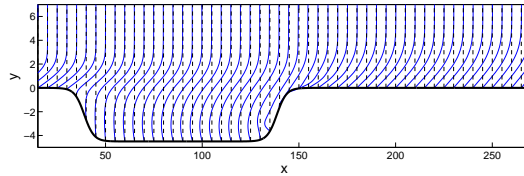

Figure 2   Streamwise base flow profile used for stability analysis and eigenmodes computation. One sees clearly the recirculation zone inside the cavity

4.2   Spectra and eigenvectors of the cavity flow

The least stable eigenvalues are shown in figure 3 where only eigenvalues with positive real part are represented. One sees two unstable eigenmodes (with positive imaginary part), with real part of about 0.15. These two modes belong to a branch, composed by the least stable eigenmodes (including modes labelled (m1), (m2) and in the sub-branch, (m3). The eigenvectors corresponding to this branch present common features, and are related to the flow around the cavity zone. Slightly more damped, we see another branch of modes with common features corresponding to modes beginning in the cavity and extending further downstream.
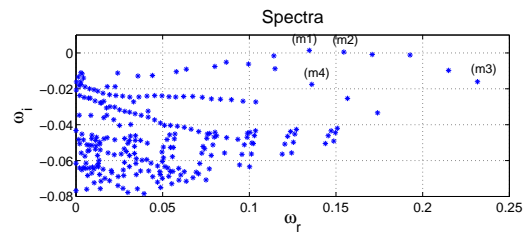

Figure 3   Eigenvalues of the cavity flow. One sees two unstable modes with imaginary part about 0.15.

The least stable eigenmode is depicted in figure 4. The streamwise and normal velocity (a) and the pressure (b) are presented. This mode mainly

consist of vortices travelling downstream the shear layer. Further analysis shows that its amplitude is growing exponentially along the shear layer, with a growth rate similar to a Kelvin-Helmholtz wave with same wave length. The velocity components for the adjoint eigenvector is presented in figure 4 (c). Regions of large amplitude of the adjoint mode indicate spatial locations where the mode is sensitive to excitations. In this case, we observe high sensitivity at the upstream lip, close to the wall. This is natural, since a forcing at this location will directly excite the shear layer instability.
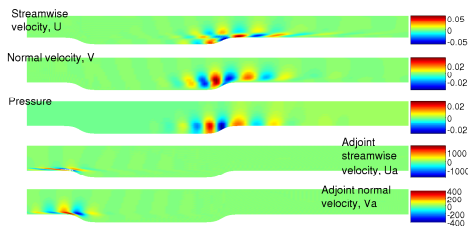

Figure 4   Least stable eigenmode, corresponding to the eigenvalue labelled *m1* in figure 3. a) streamwise and normal velocity, b) pressure, c) velocity components of corresponding adjoint eigenmode

4.3   Transient energy growth

The computation of the worst case initial condition is based on the reduced model composed of the computed eigenmodes. To see how the eigenmodes contribute to this growth, we perform the analysis with one eigenmode, then two, progressively increasing the number of included eigenmodes, beginning with the least stable ones. The obtained envelopes are depicted in figure 5. The curve with lowest energy correspond to one mode, then two modes, and up to the most energetic one with all (300) modes included. Using one mode we observe as expected an exponential growth. Using two modes, we see on top of the exponential growth, a cycle of growth and decay of period approximatively 300 time units. Increasing the number of modes, we observe the same cycle with higher energy. Finally, the envelope consist of an exponential growth much faster that the one due to the unstable modes, then the cycle, and still we can observe the effect of an exponential growth of the order of the one of the unstable modes. We will next analyse the reasons for this behaviour by inspecting the evolution of the flow field.

For each time of the envelope, there is a potentially different *worst case* initial condition. In this case, we found that all the initial conditions were resembling a wave packet in the upstream region of the shear layer, as depicted
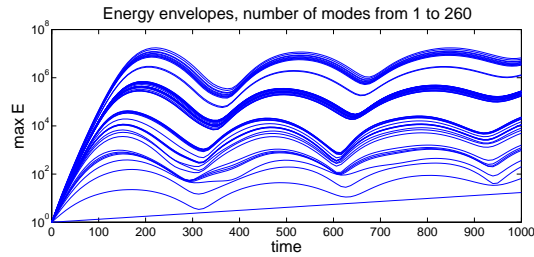
Energy envelopes, number of modes from 1 to 260

Figure 5 Envelope of maximum energy growth from initial conditions. The different lines correspond to increasing number of eigenmodes included in the optimization, 1 to 300 from bottom to top.

in figure 6. It is a common feature of convectively unstable flows that the initial condition leading to the largest energy growth is a wave packet in the upstream region of the unstable zone, see Ehrenstein & Gallaire (2005) for the worst case initial condition in the 2D Blasius boundary layer, or Cossu & Chomaz (1997); Chomaz (2005) for the Ginzburg–Landau equation.
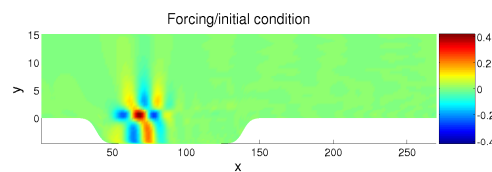

Forcing/initial condition

Figure 6 The worst case initial condition for energy growth when including 200 modes in the optimization. It corresponds to time 200 of the most energetic envelope of figure 5. The initial condition is a wave packet in the upstream region of the shear layer. The wave packet is represented at time 20 of its evolution, so that its features are more easily recognizable.

We can analyse the flow evolution due to the worst case initial condition by an x/t diagram as shown in figure 7 a) for the velocity components and b) for the pressure. One sees the convection of the initial wave packet passed the shear layer and the downstream cavity lip, and the re-apparition of the wave packet at the upstream cavity lip. When the wave packet, having grown along the shear layer, reaches the downstream cavity lip, there is a global pressure change, visible in the form of a vertical ray, regenerating a wave packet by a receptivity mechanism at the upstream cavity lip. The location of the cavity lips and wave packet propagation are underlined by black lines to put in evidence the locations of reflection and receptivity.
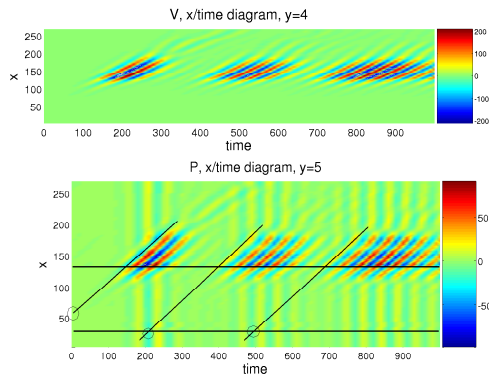
Figure 7   streamwise/time diagram of a) the normal velocity and b) the pressure in the free-stream, at $y = 4$ for the worst case initial condition. The propagation of the wave packet with group velocity approximatively 0.3 can be seen by the oblique rays in a) and b) , and the global changes of pressure are seen by the vertical rays in pressure b).

5 Feedback control using a reduced model

5.1 Control and estimation

The general setting for control is the following: the signal r is measured in the flow, in our case we chose to measure the wall shear stress at the downstream cavity lip, and an actuator is implemented with signal u. When control is active, the actuation signal is a function of the measured variable. The flow is disturbed by the external sources of excitation w, for instance acoustic waves, incoming eddies... The control objective consists in minimizing the variance of the flow state q.

In the following we will aim at minimizing the flow energy, while maintaining a small control effort. This can be expressed by the control objective function

$$\mathcal{J} = \int_0^\infty (q^H Q q + \ell^2 u^2)\mathrm{d}t \tag{2}$$

where the flow kinetic energy $\langle q, q \rangle = q^H Q q$ is accounted for, along with the control effort penalized by a control penalty ℓ.

The system is exposed to external sources of disturbance, the input w. We will represent these inputs by stochastic variables with given covariance. The stochastic input variable will be assumed uncorrelated in time, i.e. white noise.

The flow system that we aim at controlling can be described in the state space form

$$\left.\begin{aligned}\dot{q} &= Aq + B_1 w + B_2 u \\ r &= Cq + g\end{aligned}\right\} \tag{3}$$

with dynamic matrix A from the linearized Navier–Stokes equation in the 2D domain with cavity, w are stochastic external disturbances, representing for instance acoustic waves, incoming eddies or free-stream turbulence. The operator B_1 describes how these disturbances enter the dynamic equation, for instance their spatial location in the flow domain. The control input u comes as a forcing to the dynamic equation, and B_2 describes the actuators, for instance blowing and suction as a boundary condition, and spatial location of the actuator. A measurement r can be extracted from the flow state, as described by operator C. It can for instance extract the wall-shear stress at a given wall location. The measurement is disturbed by a stochastic measurement noise g with given variance.

One of the most widely used controller based on optimization is the linear quadratic Gaussian (LQG) controller. It can be decomposed in the computation of an optimal estimator, that builds an estimate of the instantaneous flow field using the available measurements, and the optimal controller for which it is assumed that the state is known exactly. The estimation and control feedback gains L and K can be computed by the solution of two Riccati equations. For description of this methodology, see e.g. Skogestad & Postlethwaite (2005), and for applications of this methodology to fluid mechanics , see e.g. Högberg *et al.* (2003*b*).
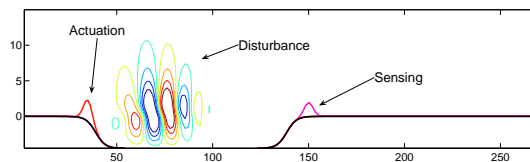

Figure 8   Sketch of the control setting. One actuator applying blowing and suction is located at the upstream lip of the cavity, and one sensor measuring wall shear stress u_y is located at the downstream lip of the cavity. The flow is excited by a random forcing in the upstream region of the shear layer.

5.2   Galerkin projection for system order reduction

The eigenmodes of the system can be used as a model for the flow dynamics. We compute about 300 pairs of leading eigenmodes. This number is still rather large for control design, and especially would be too large for a real

application, where the controller has to be run in parallel to the real flow. We have the freedom to pick out of these computed modes a set on which to project the dynamic system (3).

For projection of the dynamic system on the chosen set of eigenvectors, we can use the bi-orthogonality property of the adjoint eigenmodes. It is an easy task to project the dynamic matrix A since in the basis of eigenmodes, the dynamic operator is the diagonal matrix of the eigenvalues. Projection of the input and output operators requires more care. The relation between the physical flow state q and its expansion coefficient representation k is

$$q = \sum_i q_i k, \quad k_j = \left\langle q, q_j^+ \right\rangle. \tag{4}$$

where q_i is a single eigenmode. Applying the inner product on both sides of (3) we obtain

$$\dot{k}_j = \left\langle \dot{q}, q_j^+ \right\rangle = \left\langle A \sum_h q_h k_h, q_j^+ \right\rangle + \left\langle B_1 u, q_j^+ \right\rangle + \left\langle B_2 w, q_j^+ \right\rangle$$
$$= \omega_j k_j + \underbrace{\left\langle B_1, q_j^+ \right\rangle}_{B_1 j^M} u + \underbrace{\left\langle B_2, q_j^+ \right\rangle}_{B_2 j^M} w. \tag{5}$$

For the measurement we have

$$r = C \sum_h C q_k k_h = \sum_h \underbrace{C q_k}_{C_k^M} k_h. \tag{6}$$

The final system model is thus

$$\left.\begin{aligned} \dot{k} &= A^M k + B_1^M u + B_2^M w \\ r &= C^M k + g. \end{aligned}\right\} \tag{7}$$

The projection of the objective function is obtained by similar steps

$$\mathcal{J}^M = \int_0^\infty (k^H Q^M k + \ell^2 u^2) \mathrm{d}t, \quad \text{with } Q_{i,j}^M = q_i^H Q q_j. \tag{8}$$

If the leading eigenmodes correctly represent the system's dynamics, this reduced system will be a good model for the effect of actuation and measurement, and the reduced energy measure Q^M, will be a good measure of the flow kinetic energy, and thus of the control performance.

6   Results

For the control results presented in this section we have chosen the following design parameters. The actuation signal penalty ℓ was chosen 10^8. This high

value is to be compared to the flow energy term in the objective function (2). Since the energy is high and the actuation penalization is a relative term, we need a high penalty ℓ. The sensor noise term was chosen as 8×10^3. Once again, this high term should be compared to the large flow mean energy achieved to the external source of excitation w.

6.1 Control and estimation gains

The estimation gain computed with the chosen parameters are represented in figure 9(a). Its support is located in the region of the shear layer, with an amplitude growth comparable to that of the cavity eigenmodes. The control gain can be seen in figure 9(b). Its support is located upstream of the cavity, close to the wall. the actuator signal is computed as the inner product of the control gain with the estimated flow state $u(t) = \langle K, \hat{q}(t) \rangle$.
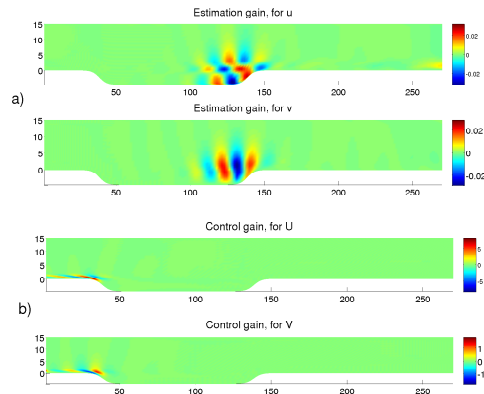

Figure 9 The control gain K (a) and estimation gain L (b), represented by their streamwise and normal components. For control, the actuator signal $u(t)$ is obtained by evaluation of the inner product $u(t) = \langle K, \hat{q}(t) \rangle$ where $\hat{q}(t)$ is the estimated flow state. For estimation, the estimated flow state is forced with forcing function $L(r(t) - \hat{r}(t))$ where the term $r(t) - \hat{r}(t)$ denotes the measurement mismatch between the flow and the estimated flow

The state space representation of the controller system has several states, but have a single input and single output (SISO). In this context, it is interesting to represent the transfer function of the controller by its impulse response i.e. the actuation signal that would result from an impulse at the measurement. This impulse response is represented in figure 10. This impulse response can also be interpreted as a convolution kernel for the measurement

signal history to obtain the actuation:

$$u(t) = \int_0^\infty \mathcal{G}(\tau) r(t - \tau) \mathrm{d}\tau \tag{9}$$

One can see from figure 10 that the measurement history up to 300 time units in the past is necessary for control. This time corresponds well with the cycle period found in previous sections.
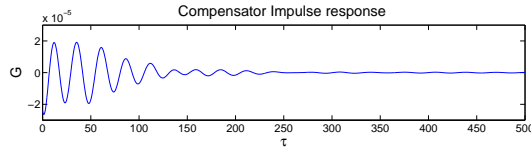

Figure 10 Actuation signal at the output of the controller for an impulse at the measurement. Can as well be interpreted as a convolution kernel to obtain the actuation signal from past measurements.

6.2 Controlled flow

To test the control performance, we implement an oscillating volume force in the upstream region of the shear layer in the DNS simulation. Its spatial structure is chosen as the worst case initial condition found in §4.3. We then compare the energy evolution for the controlled and uncontrolled flow as represented in figure 11.

One can recognize in figure 11 the energy cycles similar to the response to the worst case initial condition in §4.3. In fact the oscillating force have a very similar effect on the flow dynamics, since it most affects the flow when it is turned on. For the controlled flow, one observes the same energy growth for its first peak, and after the first decay, no energy growth is observed.

While the wave packet is convected along the shear layer, there is no control authority, since the actuator is located upstream, but at the time the perturbation reaches the downstream cavity lip, it can be sensed, and the actuator can play its role, counteracting the receptivity to pressure and thus the regeneration of the wave packet.

This mechanism can be observed in more details in figure 12 where x/t diagram similar as to §4.3 represent the flow and controlled flow evolution at $y = 4$ for the normal velocity and the pressure. When control is applied, one naturally still observes the vertical rays of the global pressure changes, but the wave packet does not reappear.
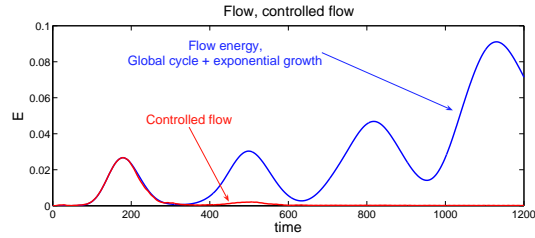
Figure 11 Flow energy when excited with oscillating volume force in the upstream region of the shear layer with (*dashed*) and without control (*solid*) . One sees the energy cycles for the uncontrolled flow. For the controlled flow, only the first growth cycle is still present: the controller has prevented the regeneration of the wave packet.
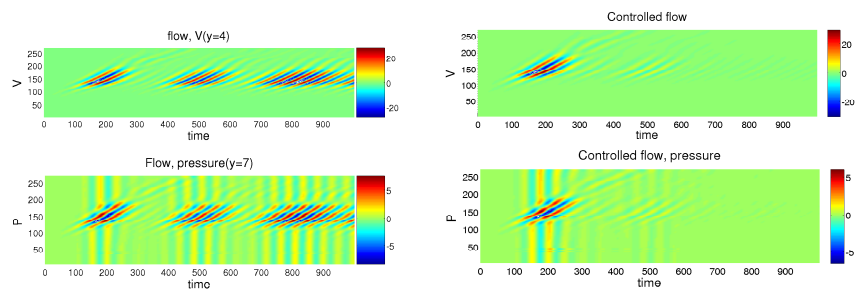

Figure 12 x/t diagrams for the flow normal velocity and pressure in the case a) without control, and b) with control. The vertical rays of the pressure variation is still visible, but the wave packet regeneration is prevented.

7   Conclusion

In this paper, we have applied feedback control on a two dimensional flow using the flow's eigenmodes to build a reduced order model. The control methodology was the LQG (Linear Quadratic Gaussian), the eigenmodes of the large system was computed by means of a Krylov/Arnoldi method. The flow composed of a recirculating cavity was found to be unstable due to a pressure feedback mechanism between the re-attachment and detachment points of the cavity flow. The controller based on the 20 least stable eigenmodes of the system was found to perform well on a Galerkin model of the cavity flow constructed using all the computed eigenmodes (300 pairs). We found that the self-sustaining process due to the pressure was removed by the controller. The next step is to apply the controller computed using the least stable eigenmodes to the full direct numerical simulation of the flow.

Bibliography

CHOMAZ, J.-M. 2005 Global instabilities in spatially developing flows: non-normality and nonlinearity. *Annu. Rev. Fluid Mech.* **37**, 357–392.

COSSU, C. & CHOMAZ, J.-M. 1997 Global measures of local convective instabilities. *Physical review letters* **78** (23), 4387–4390.

EDWARDS, TUCKERMAN, FRIESNER & SORENSEN 1994 Krylov methods for the incompressible navier-stokes equations. *J. Comput. Phys.* **110**, 82–102.

EHRENSTEIN, U. & GALLAIRE, F. 2005 On two-dimensional temporal modes in spatially evolving open flows: the flat-plate boundary layer. *J. Fluid Mech.* **536**, 209–218.

HUERRE, P. 2000 *Perspective in fluid dynamics*, chap. Open shear flow instabilities, pp. 159–229. Cambridge university press.

HÖGBERG, M., BEWLEY, T. & HENNINGSON, D. 2003*a* Relaminarization of Re_τ=100 turbulence using gain scheduling and linear state-feedback control. *Physics of fluids* **15**, 3572–3575.

HÖGBERG, M., BEWLEY, T. R. & HENNINGSON, D. S. 2003*b* Linear feedback control and estimation of transition in plane channel flow. *J. Fluid Mech.* **481**, 149–175.

HÖGBERG, M. & HENNINGSON, D. S. 2002 Linear optimal control applied to instabilities in spatially developing boundary layers. *J. Fluid Mech.* **470**, 151–179.

KIM, J. 2003 Control of turbulent boundary layers. *Physics of fluids* **15** (5).

MARQUILLIE, M. & EHRENSTEIN, U. 2003 On the onset of nonlinear oscillations in a separating boundary-layer flow. *J. Fluid Mech.* **490**, 169–188.

NAYAR, M. & ORTEGA, U. 1993 Computation of selected eigenvalues of generalized eigenvalues problems. *J. Comp. Phys.* **108**, 8–14.

OBINATA, G. & ANDERSON, B. D. 2001 *Model reduction for control system design*. Springer.

ROWLEY, C., COLONIUS, T. & BASU, A. 2002 On self-sustained oscillations in two-dimensional compressible flow over rectangular cavities. *J. Fluid Mech.* **455**, 315 – 346.

SCHMID, P. J. & HENNINGSON, D. S. 2001 *Stability and transition in shear flows*. Springer.

SKOGESTAD, S. & POSTLETHWAITE, I. 2005 *Multivariable feedback control, Analysis and Design, 2nd edition*. Wiley.

THEOFILIS, V. 2003 Advances in global linear instability analysis of non-parallel and three-dimensional flows. *Progress in aerospace sciences* **39**, 249–315.